The effect of shock waves on diamagnetic fabrics

Sonal Tiwari[1], Amar Agarwal[1], Thomas Kenkmann[2], Michael H. Poelchau[2]

[1]Department of Earth Sciences, Indian Institute of Technology-Kanpur, Kanpur – 208016, India.

[2]Geology, University of Freiburg, 79104 Freiburg, Germany

Corresponding author´s email: amar@daad-alumni.de

Abstract

Para- and ferro-magnetic fabrics are known to provide essential clues for understanding impact cratering processes. However, research on the effects of shock waves on diamagnetic fabrics is lacking. We, therefore, conducted a hypervelocity impact experiment on a block of diamagnetic Taunus quartzite and studied the changes in diamagnetic fabrics. In the crater subsurface, the reorientation of the diamagnetic fabrics is concentrated in a zone of ~4 projectile diameters (25 mm) width directly below the point of impact. Higher reorientation in this zone indicates the concentration of damage. We argue that although the shockwaves traversed through the target with a hemi spherical wavefront, the damage was concentrated directly below the point of impact.

Another important observation is that the weak shock waves have changed the diamagnetic parameters. The bulk susceptibility has increased overall, while the corrected degree of anisotropy (P') and the shape parameter (T) have increased in the crater subsurface but have decreased at the target surface. We propose that the variable response of P' and T could be due to the difference in incident angle subtended by the shock wave on the diamagnetic foliation at the target surface (c. 34°) and in the subsurface (c. 54°). These results, thus, show that the changes in diamagnetic fabrics can be used as a proxy for plastic deformation caused by shock waves at low peak pressures.

Keywords

Experimental impact cratering, MEMIN, diamagnetic fabrics, quartzite, low shock pressures

1. Introduction

Quantification of the deformation in the crater subsurface is vital for understanding the processes active during impact cratering. These subsurface processes govern the final crater morphology and pave the way for hydrothermal systems that act as a cradle for new life (Cockell & Lee, 2002) and form ore

deposits (Grajales-Nishimura et al., 2000; R. A. F. Grieve & Masaitis, 1994; Richard A F Grieve, 2005; Masaitis, 1998; Reimold et al., 2005). Laboratory shock experiments that mimic the natural conditions are a method to investigate the subsurface deformation at different impact settings (Greeley et al., 1980, 1982; Kenkmann et al., 2018; Lange et al., 1984; Melosh, 1980; Oberbeck, 1971; Schultz et al., 2007). Investigating experimental craters has inherent advantages of controlled projectile and target properties and that they are not weathered and eroded.

Anisotropy of magnetic susceptibility (AMS) is a measure of the intensity and orientation of the magnetic fabrics. Change in AMS, with distance from the point of impact in natural and experimental craters is an excellent yard-stick of shock-induced deformation (A. Agarwal & Alva-Valdivia, 2019; Amar Agarwal et al., 2015, 2016; Amar Agarwal, Kontny, et al., 2019; Elbra et al., 2009; Gattacceca et al., 2007; A.M. Hirt et al., 1993; Muxworthy et al., 2017; Scott & Spray, 1999; Urrutia-Fucugauchi et al., 2012; Yokoyama et al., 2012). AMS has been used as a strain gauge in tectonites, and for shock barometery and shock wavefront reconstruction in impactites (G. Borradaile & Alford, 1987; G.J. Borradaile & Henry, 1997; G J Borradaile, 1987; Graham John Borradaile, 1988; Burmeister et al., 2009; Ferré et al., 2014; Gattacceca et al., 2007; Itoyuki Nishioka et al., 2007).

Notably, all the AMS investigations of impactites, natural or experimental, have been limited to ferromagnetic and paramagnetic target rocks with Fe-oxides and micas as carrier minerals. However, there are many impact craters with quarzitic or calcitic target rocks, such as the Malmian Limestone at Ries Crater, Germany, the Coconino sandstone at the Meteor Crater, USA, and the Bhander Sandstone of Ramgarh Crater, India (Kenkmann et al., 2020; Kieffer, 1971; Pohl et al., 1977). Furthermore, quartz is the most important rock-forming mineral, which presents a diamagnetic behaviour and is abundant on the crust of Earth and other planetary bodies.

Microstructures and transformations in quartz form the backbone of peak shock pressure determination (shock barometry) and provide crucial proof of a meteoritic impact (French & Koeberl, 2010; D Stöffler, 1972; Dieter Stöffler et al., 2018; Dieter Stöffler & Langenhorst, 1994). However, these shock barometers and proofs of impact exist only for pressures over 5 GPa. It is pretty challenging to determine peak pressures and identify evidence of impact cratering in rocks that experienced pressures below 5 GPa using microstructures. This is perhaps, due to the lack of unique and identifiable shock microstructures. On the contrary, preliminary investigations of changes in magnetic fabrics, of natural and experimental craters, at low shock pressures (< 5 GPa) has shown encouraging results (A. Agarwal & Alva-Valdivia, 2019; Amar Agarwal et al., 2015, 2016; Amar Agarwal, Kontny, et al., 2019; Gattacceca et al., 2007; I Nishioka & Funaki, 2008; Itoyuki Nishioka et al., 2007). Moreover, AMS has been regularly used to identify, otherwise inconspicuous, tectonic deformation in weakly deformed rocks (Amar Agarwal et al., 2021; Graham J. Borradaile &

Tarling, 1981; Cifelli et al., 2004; Kissel et al., 1986; Parés, 2004; Soto et al., 2009).

Therefore, we investigate the changes in the magnetic fabrics of Taunus quartzite due to experimental impact cratering at low shock pressures, where other common shock microstructures are absent. We have selected Taunus quartzite for this study because it is diamagnetic, and its mineralogical and mechanical characteristics are well established (Moser et al., 2013; Poelchau et al., 2014). The first objective of this spatially resolved AMS investigation of to understand the change in the diamagnetic fabrics at the target surface and subsurface with distance from the experimental point of impact. The second objective is to identify the differences in effects of shock waves in the crater subsurface to that at the target surface. Based on the results, we argue that the diamagnetic fabrics show characteristic effects of shock-induced deformation, which may be used as a proxy for deformation. This study thus contributes to the understanding of the subsurface deformation at impact craters and adds to the currently under investigated effect of stresses (tectonic, seismic, shock wave led) on diamagnetic fabrics.

1.1 Magnetic fabrics in rocks containing mostly quartz

Special care must be taken while interpreting diamagnetic fabrics. The magnetic susceptibility of quartz single-crystal is diamagnetic (-14 $\times$ 10^{-6} SI units), and it exhibits only very small anisotropy, mostly less than 1% (Hrouda & Kapička, 1986). Moreover, in some cases, the susceptibility along the c (trigonal) axis is higher than that in the ab plane, and in other cases, it is lower (Hrouda & Kapička, 1986). Diamagnetic properties dominate when diamagnetic minerals (quartz and calcite) form more than 80% of the rock (Tarling & Shi, 1995). The addition of a very small para- or ferromagnetic component may render the rock as para- or ferromagnetic (Ann M. Hirt & Almqvist, 2012). Such addition can be identified by the high corrected degree of magnetic anisotropy (*P'*) and bulk susceptibility approaching zero (Ferré, 2002; Ann M. Hirt & Almqvist, 2012; Lüneburg et al., 1999; Rochette, 1987).

There are two approaches to describe diamagnetic AMS (Hrouda, 2004). The first approach is similar to that in para- and ferromagnetic fabric. For negative susceptibilities, the largest absolute magnitude is the minimum susceptibility k_1, and the smallest absolute magnitude is the maximum susceptibility k_3, where k_1 k_2 k_3. The second approach considers the non-signed values of the principal susceptibilities. Here, the strongest diamagnetic susceptibility, with the largest magnitude, is the absolute value of the maximum susceptibility k_3, while the minimum susceptibility corresponds to the smallest absolute magnitude susceptibility, where k_3 k_2 k_1. The first approach is best for plotting the principal directions, as the magnetic foliation parallels the petrographic foliation. The second approach is best for characterizing the *P'*, magnetic lineation, magnetic foliation and the shape of the susceptibility ellipsoid (Hrouda, 2004). This study compares the changes in the magnetic fabrics among specimens within the spec-

imen frame of reference and thus, utilizes the second approach.

2. Material and methods

2.1 Target Material

Taunus quartzite was quarried by the Taunus-Quarzit-Werke GmbH & Co. KG, Wehrheim, Germany (Fig. 1). The physical and mineralogical properties of Taunus quartzite was detailed in previous reports (Moser et al., 2013; Poelchau et al., 2014; Winkler et al., 2018). The Taunus quartzite was formed by a low-grade Variscan metamorphosis that overprinted a 405 Ma sandstone. It consists of ~91 vol% quartz and ~8 vol% fine-grained mica-bearing matrix along with small amounts of rutile, chromite, zircon and monazite. The original sedimentary layering is faint but discernible. Millimetre thick, green-coloured phyllosilicate layers are interspersed through the blocks. The sedimentary porosity has been filled by a matrix of µm-sized quartz and muscovite grains. With a density of 2.62 ± 0.02 g/cm^3, the average porosity lies below 1%. The uniaxial compressive strength is 292 MPa, and the tensile strength is 16.7 MPa (Poelchau et al., 2014). The P-wave velocity determined by Moser et al. (2013) on 20 cm cubes is 4.98 ± 0.07 km/s.

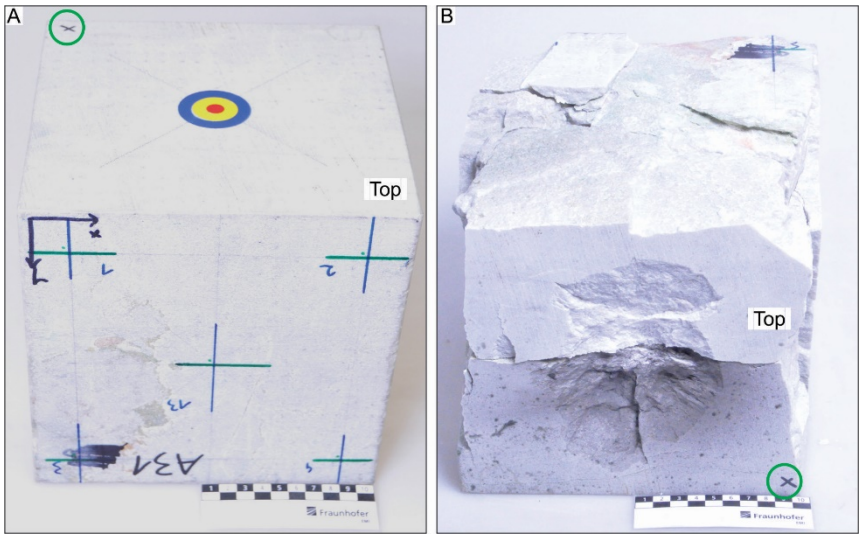

Fig. 1 (A-B). Photographs of the Taunus quartzite block (20 x 20 x 20 cm) before and after the impact experiment. The block was broken into several pieces after the experiment. The top/target surface is marked with "Top" and "X" inside a green circle. Note the different orientations of the block in the two images.

2.2 Experimental cratering

A cube of Taunus quartzite with 20 cm long edges was used for the impact cratering experiment (Fig. 1). The experiment was carried out with a two-stage light-gas gun with an 8.5 mm calibre launch tube at the Fraunhofer Ernst-Mach-Institute for High-Speed Dynamics (EMI) in Freiburg (EMI), Germany. The projectile diameter (d_p) was 6.18 mm. The projectile, a 0.3690 g basalt sphere, was accelerated to 5.457 kms^{-1} and the target chamber pressure was 1.2 mbar. For details of the accelerator and the exact experimental assembly, refer to Schneider and Schäfer (2001), Poelchau et al. (Poelchau et al., 2014) and Kenkmann et al. (Kenkmann et al., 2018). After the experiment, the crater cavity was impregnated with low-viscosity epoxy to preserve porosity and microstructures.

The calculated equivalent depth of burst, i.e., the point source, is defined as:

$$d_b = d_p \sqrt{\frac{\rho_p}{\rho_t}}$$

Where d_p is the projectile diameter, $_p$ is the projectile density, and $_t$ is the target density (Birkhoff et al., 1948). The point source of the shock waves is, thus, at a depth of 2.7 mm.

2.3 Measurements of magnetic fabrics

A nonmagnetic diamond bit, 14 mm in diameter, was used to drill oriented cylindrical cores from the unshocked and shocked Taunus quartzite blocks. Nine cylinders were drilled from the unshocked block. Each cylinder was cut precisely to produce one standard rock magnetic specimen, which is 14 mm in diameter and 11.2 mm long. Thus, a total of 9 unshocked specimens were recovered. The target blocks were bisected through the crater centre, and twelve cylinders each were drilled from the 'target surface' and 'subsurface' (Fig. 2). Each cylinder was cut precisely to produce two standard rock magnetic specimens. Twenty-four specimens were, thus, recovered from the target- and sub-surface, each. Specimens 5.1 to 5.24 from the target surface and 6.1 to 6.24 from the subsurface. Specimens 5.1 to 5.12 and 6.1 to 6.12 are from the top part of the cylinders, while specimens 5.13 to 5.24 and 6.13 to 6.24 are from the bottom part of the cylinders (Fig. 2). The magnetic fabrics are represented in the sample coordinate system, such that the half-arrows at the target surface are supposed to point towards the north (Fig. 2).

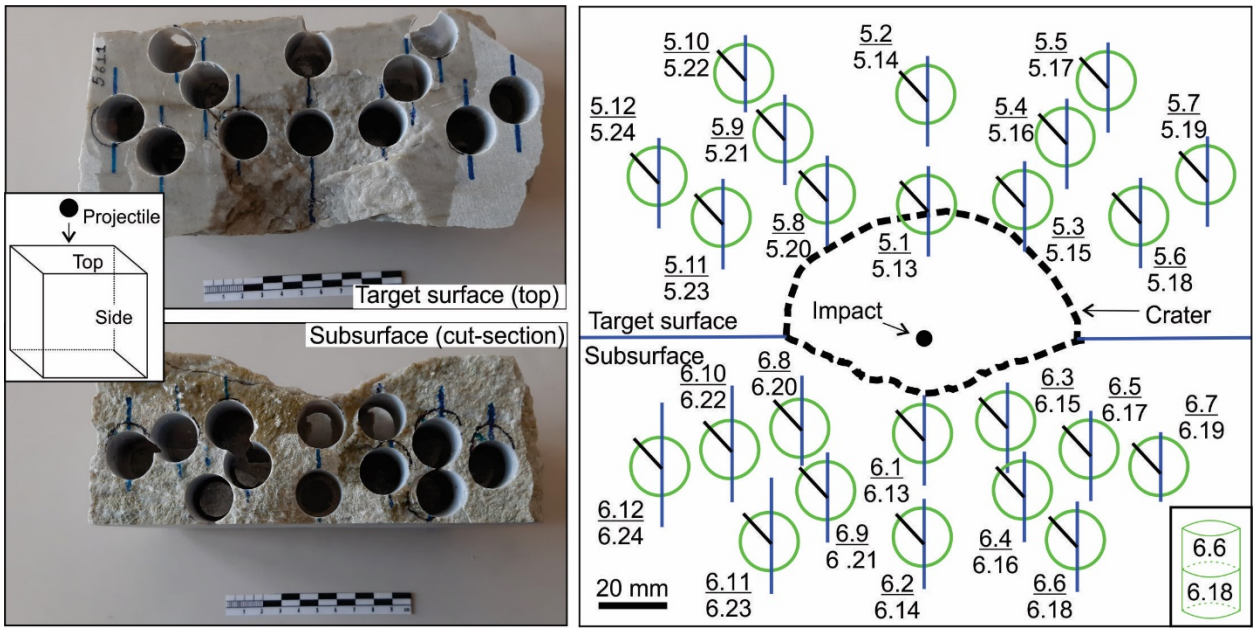

Figure 2. The photographs and sketches show the drilling position with respect to the impact crater. In the sketch: black circles in the centre mark the estimated point of impact. The green circles represent the exact position of the drilled cylinders, and the half-arrows mark the "north" of the specimen coordinate systems. From each core, two specimens were cut, and the upper and lower specimens are written as nominator and denominator of the fraction (see inset bottom-right).

The AMS was determined for the 9 unshocked and 48 shocked specimens at room temperature in KLY-4S Kappabridge (AGICO) using an automatic rotator sample holder. The Kappabridge has an operating frequency of 875 Hz, and the measurements were made in the spinner mode, using the SUFAR program (AGICO, Brno), in a field intensity of 300 Am^{-1}. In the spinner mode, the specimen rotates at 1 revolution per 2 s inside the coil of the Kappabridge and the susceptibility is measured 64 times during one revolution. The measurements are made along three perpendicular axes, and standard AMS parameters (enumerated below) are calculated. The sensitivity of AMS measurement in the spinner mode is 2 x 10^{-8} SI units. The data is visualized through Stereonet v.11 (Cardozo & Allmendinger, 2013).

This study uses the approach of determining the AMS, where the absolute (non-signed) values of the principal susceptibilities are considered and $k_3 \quad k_2 \quad k_1$ (Hrouda, 2004). k_3, k_2, and k_1, are thus, the maximum, intermediate and minimum principal susceptibility axes, respectively. The mean bulk magnetic susceptibility (K_m), corrected magnetic anisotropy (P'), and shape parameter (T) are, thus, given by the following formulas determined by equations by Jelenik

(1981) and Hrouda (Hrouda, 2004):

$K_m = (k_1 + k_2 + k_3)/3$

$$P' = exp\sqrt{2\left[(n_1 - n_m)^2 + (n_2 - n_m)^2 + (n_3 - n_m)^2\right]}$$

$$T = \frac{(2n_2 - n_1 - n_3)}{(n_1 - n_3)}$$

Here $n_1 = \ln k_3$; $n_2 = \ln k_2$; $n_3 = \ln k_1$; $n_m = (n_1 * n_2 * n_3)^{1/3}$. The dispersion in the orientation of the principal susceptibility axes is quantified using standard spherical statistical parameters *95* and *kappa* (Fisher et al., 1993). The confidence limit *95* is a measure of the precision with which the true mean direction has been estimated. One is 95% certain that the unknown true mean direction lies within *95* of the calculated mean. *kappa* is a precision parameter, and it approaches infinity as the dispersion goes to zero.

2.4 Hysteresis measurements

After the AMS measurements, small pieces of the specimens were broken for measuring the hysteresis behaviour. Hysteresis reveals the prominent magnetic behaviour and dominant domain state of the magnetic carriers (Day et al., 1977). Determination of the dominant magnetic behaviour is critical as the diamagnetism of rocks is transformed to para- or ferromagnetism with the addition of the smallest proportions of para- and ferromagnetic minerals, respectively. In total 12 specimens, 3 unshocked (1, 3 and 10) and 9 shocked (5.1, 5.8, 5.13, 5.15, 5.24, 6.13, 6.18, 6.20 and 6.23) were analysed. The hysteresis was analyzed through a Microsense Vibrating Sample Magnetometer (VSM) in the applied field up to 1.75 T at room temperature, using increments of 0.1 T.

2.5 Microscopy

After the AMS measurements, the cylindrical specimens were cut to make thin sections. We prepared 24 thin sections each from the target and the subsurface. The pre and post impact microstructures of the unshocked and shocked samples were studied under a Leica DM4 scanning optical microscope.

3. Results

3.1 Pre-impact microstructures

The subhedral to anhedral crystals of quartz gives hypidiomorphic and interlocking texture (Fig. 3A). Their average grain size is 100–200 µm. The quartz crystal shows both patchy undulose extinction (Fig. 3B). The long dimension of the quartz ranges from 0.1- 1.2 mm. Serrated grain boundary, grain boundary

migration, Boehm lamellae and recrystallized quartz (salt and pepper texture) are common (Fig. 3B). In few thin sections (Fig. 3C), the stretched quartz grains form ataxial veins, which are formed due to the repeated fracturing and growth of grains, during deformation (Passchier and Trouw, 2005).

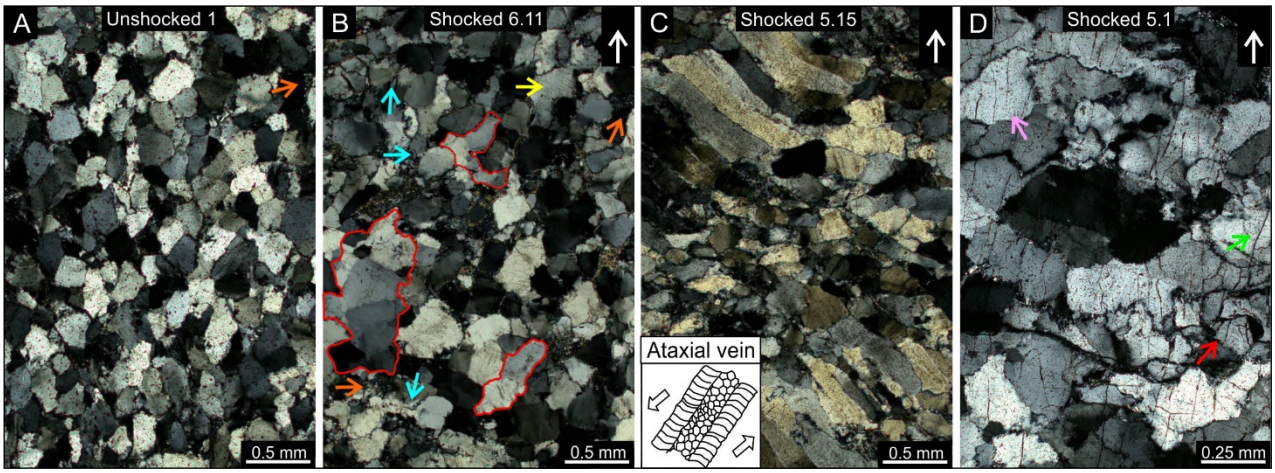

Figure 3. Cross polarised images of unshocked (A) and shocked (B, C, D) samples. Most common microstructures, which represent the metamorphic event are quartz showing patchy undulose extinction, recrystallized quartz (orange arrows), serrated grain boundaries, grain boundary migration (blue arrows), Bohem lamellae (yellow arrow), sub grains (marked with red boundary) and ataxial veins formed by stretched quartz crystals. Brittle deformation from impact experiment is realised as intragranular (pink arrow), transgranular (green arrow) fractures, some of which are open tensile microfractures (red arrow).

3.1.2 Impact induced microstructures

The quartz grains from target surface and subsurface the show trans- and intragranular microfractures, without secondary filling. At the target surface the tensile with concentric and radial orientation are common. The concentric fractures cross-cut the radial fractures (Fig. 3D), which form during the decompressive phase and compressive phase of the shock wave, respectively (Amar Agarwal et al., 2015; Ahrens & Rubin, 1993; Pierazzo & Melosh, 2000). In the subsurface the microfracture density is higher near the crater floor and seems to decrease with depth. We did not find micro shear zones either at the target surface or the subsurface as described by Winkler (2018).

3.2 Dominant magnetic carriers

Hysteresis loops of end-member behaviours are characteristic (e.g., Tauxe, 2003); however, natural samples are seldom pure. They often are a mixture of at least two prominent behaviours (Alva-Valdivia et al., 2017, e.g., 2019). In the present

case, a negative correlation between the applied field and the magnetization reveals a dominantly diamagnetic behaviour (Fig. 4). A typical diamagnetic curve has a negative linear slope. However, the present curves are neither linear nor have a slope of -1. Their middle part has a positive slope with S-shaped geometry indicating a minor ferromagnetic contribution.

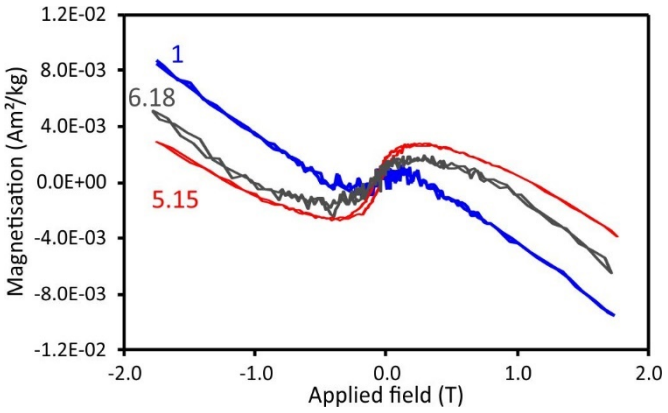

Figure 4. Representative unshocked (1-blue) and shocked (5.15-red, 6.18-grey) Taunus quartzite samples reveal a diamagnetic hysteresis behaviour with an overall negative correlation between magnetization and applied field.

3.3 Magnetic fabrics

3.3.1 Unshocked magnetic fabrics

Concurring with the overall diamagnetic behaviour in hysteresis, the mean bulk magnetic susceptibility (K_m) is -47.10 ± 1.23 x 10^{-6} SI (Table 1, Fig. 5,). Even though quartz has very low anisotropy, Tanus quartzite presents high anisotropy with 1.24 P' 1.31, average = 1.25 (Fig. 5, Table 1, supplementary table 1). This high P' may be owed to contributions from paramagnetic minerals which were observed during the microscopy. The dependence of P' on the paramagnets is underlined by its positive correlation with K_m, even though the overall behaviour is diamagnetic. The magnetic fabrics are classified as triaxial-oblate as T is consistently positive, and the three principal susceptibility axes are well clustered, with high *kappa* (Fig. 6, Table 1, supplementary table 1). On average, the *k3* plunges by 56° from the target surface. Thus, the direction of impact was oblique, at 34°, to the magnetic foliation.

Table 1: The average values of rock magnetic parameters are compiled. K_m is the mean bulk magnetic susceptibility. P' is the corrected degree magnetic anisotropy, and T is the shape factor. Note that according to the approach two of Hrouda (2004), *k1*, *k2* and *k3* are the intensities of the minimum, intermediate and maximum principal magnetic susceptibility axes, respectively. Their orientation is presented as declination (*Dec*) and inclination (*Inc*) in degrees. The confidence angle (*95*) and dispersion factor (*kappa*) are also given.

Sample	N	Km (10^{-6}) SI	P'	T	k1	k2	k3				
		Average	Std. Err.			Int	Dec	Inc	95	kappa	In
Unshocked	9	-47.1	0.0012	1.3	1.28	-0.866	304	28	0.8	3811	-1
Shocked-Target surface	24	-50.4	0.0023	1.22	1.25	-0.879	303	29	1.6	343	-1
Shocked-Subsurface	24	-44.7	0.0061	1.28	1.30	-0.856	304	28	1	1414	-1

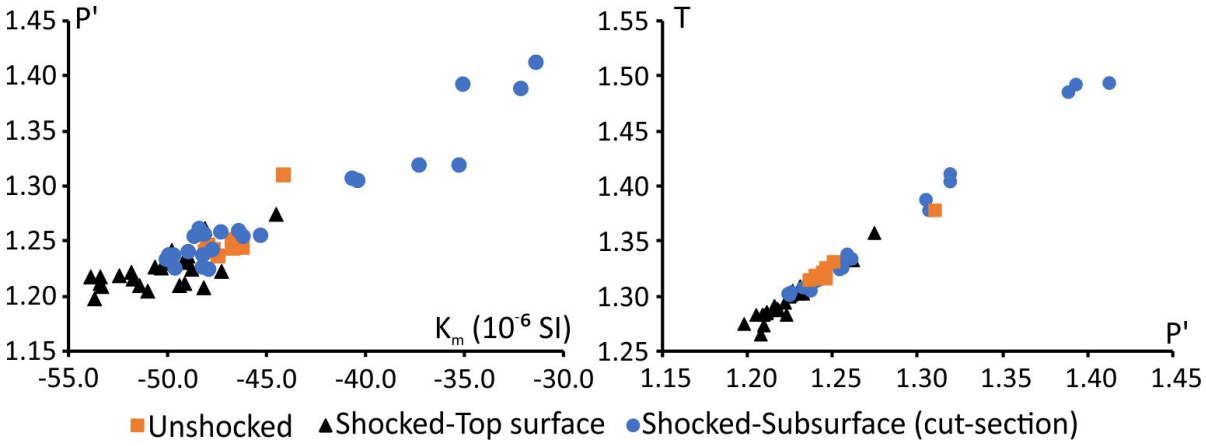

Figure 5. Graphs showing the change in corrected anisotropy (P), shape parameter (T), and mean bulk susceptibility (K_m) after the impact experiment.

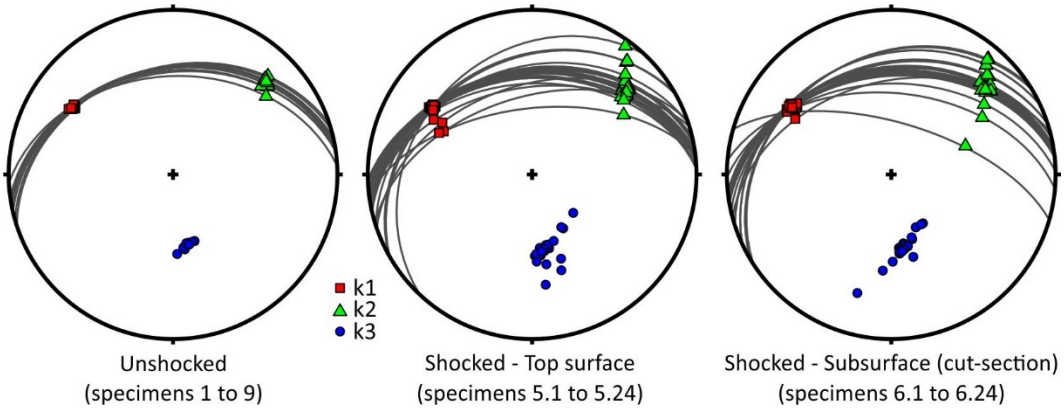

Figure 6: Lower hemisphere stereographic projections presenting the orientation of the principal susceptibility axes and the magnetic foliation in the shocked and unshocked specimens in the sample coordinate system.

3.3.2 Shocked magnetic fabrics

At the target surface, the AMS parameters of K_m, P' and T, are lower than the unshocked values. On the contrary, these parameters seem to have slightly increased in the crater subsurface (Fig. 5, table 1, supplementary table 1). In

general, the AMS parameters change more in the subsurface than in the target surface (Supplementary Fig. 1). The mean orientations of the susceptibility axes changed slightly after impact (Table 1). The susceptibility axes are more dispersed after shock, as evident from *kappa* values that are up to an order of magnitude lower than unshocked (Table 1). This dispersion has weakened the tight clustering of the axes, and the triaxial arrangement in unshocked specimens. However, the overall magnetic fabrics are still oblate ($T > 0$, Table 1). The dispersion of k_1 is highest at the target surface followed by the subsurface and least in the unshocked samples. While k_2 and k_3 are more dispersed in subsurface followed by target surface and least in unshocked samples.

The reorientation of magnetic fabrics due to the impact experiment is discussed in terms of the *k3* axis, which is the pole to the magnetic foliation (Fig. 7). The quantum of change is presented with respect to the average value calculated from the unshocked samples (Table 1). The target surface maps represent the situation at 7 and 21 mm depth from the target surface, while the subsurface maps are offset by 7 and 21 mm from the crater centre (Fig. 7). These coincide with the centre of the top (14 mm long) and the lower specimens (14 mm long).

At the target surface, the *k3* is reoriented up to 22.49° near the crater (Fig. 7a, b). The reorientation decreases with distance to 1.2° in the farthest specimens. Larger reorientations are observed in the upper specimens (5.1 to 5.12) than in the lower (5.13 to 5.24). In the subsurface, the upper specimens (6.1 to 6.12) present the largest reorientation (up to 18.8°), in the c. 4 d_p wide red zone, directly below the point of impact (Fig. 7c). The reorientation is lesser on either side of this zone. In comparison, the lower specimens (6.13 to 6.24) in the subsurface show lesser reorientation (Fig. 7d), without any recognizable pattern.

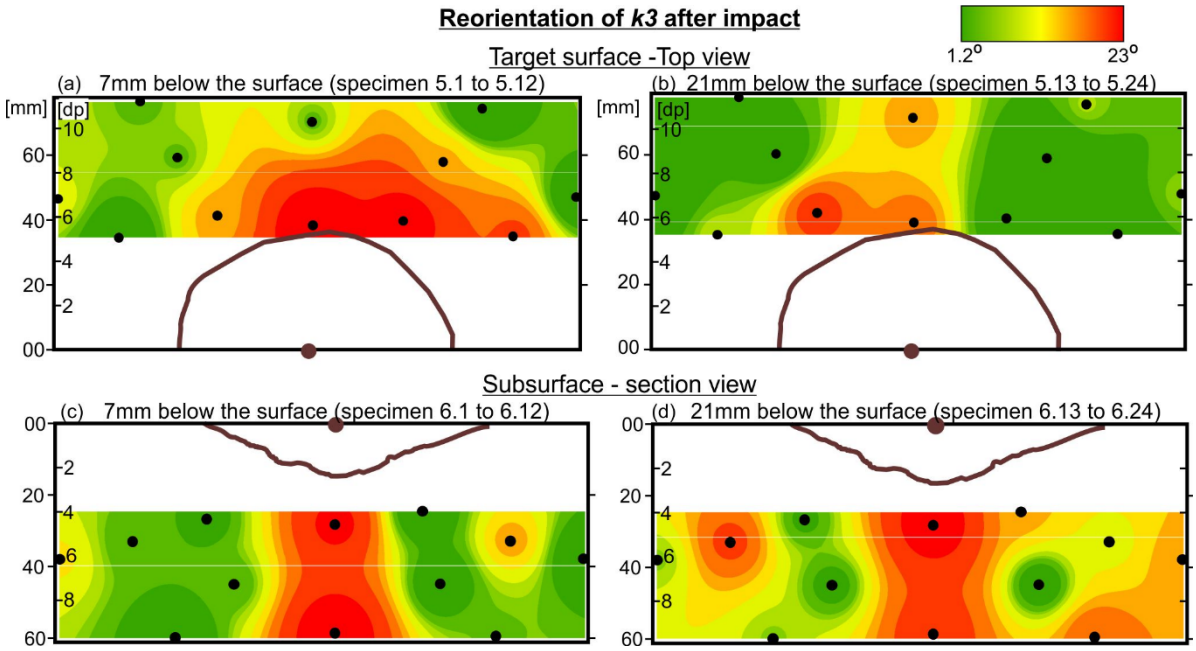

Figure 7. The images show the specimens' position (black dots), the point source (brown dot), impact crater (brown arc) and the variation in the orientation of *k3*. The target surface maps are horizontal cuts at depths of 7 and 21 mm below the target surface, marking the centre of the upper and lower set of specimens. The subsurface-view maps are vertical cuts with 7- and 21-mm offset from the crater centre, corresponding to the centre of the upper and lower set of specimens.

The damage due to shock waves decreases with distance from the point source. This phenomenon is best observed in three specimen sets that were drilled in a radial profile from the point source, namely 5.3-5.4-5.5, 5.8-5.9-5.10, and 5.15-5.16-5.17 (Fig. 2). Here specimens that are nearest to the point source, thus suffering the strongest shock waves, make the largest angles with the mean unshocked k_3. For example, in 5.3, 5.8 and 5.15, *k3* subtends angles of 16.1 $^\circ$, 8.2 $^\circ$ and 3.1 $^\circ$ with the mean unshocked *k3*, respectively; while, in 5.5, 5.10 and 5.17, *k3* make angles of 1.2 $^\circ$, 5.0 $^\circ$ and 1.2 $^\circ$, respectively (Fig. 8).

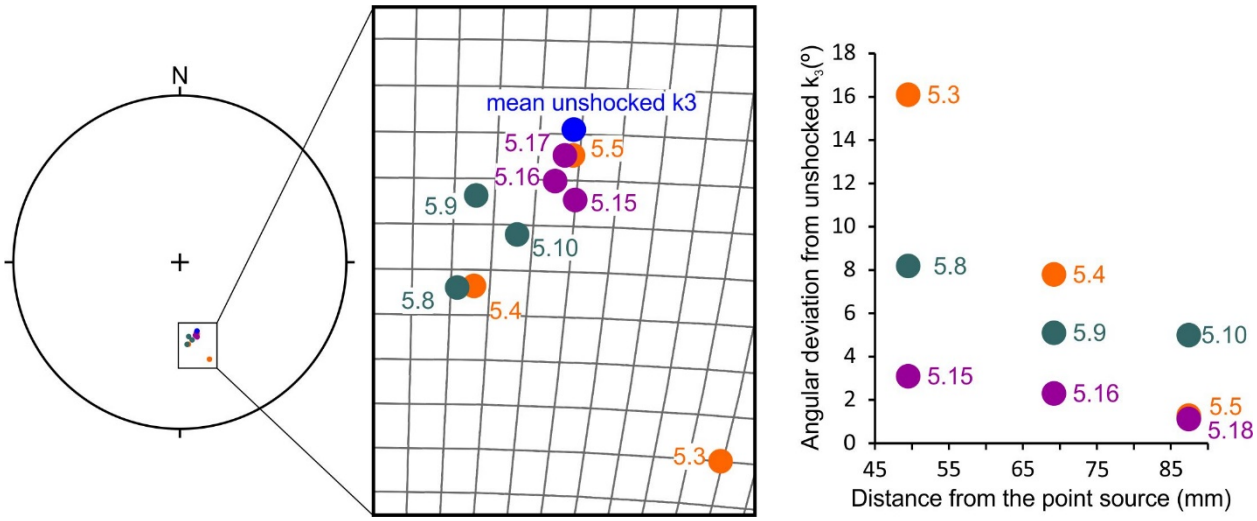

Figure 8. Systematically increasing reorientation of *k3* in shocked specimens, with respect to the mean unshocked k3, with vicinity to the point source. Three sets are shown; set 1: 5.3-5.4-5.5, set 2: 5.15-5.16-5.17 and set 3: 5.8-5.9-5.10.

4. Discussions

A hypervelocity impact experiment was done on a block of diamagnetic Taunus Quartzite. In other experiments with similar projectile properties and impact velocity, the shock pressure was calculated to be over 50 GPa at the point of impact (Amar Agarwal, Poelchau, et al., 2019). However, the pressure rapidly decreases with distance from the point source, and the subsurface of the craters experiences low shock pressures (< 3 GPa), which falls in S0–S1 of the typical shock stage classification (Dieter Stöffler et al., 2018). At such low pressures, shock indicators and barometers are not well constrained. Shock barometers are better established for higher shock pressures (> 5 GPa). The present study, therefore, looks at the changes in magentic fabrics of quartz after experiemntal impact deformation.

4.1. Effect of shock waves on diamagnetic AMS parameters

The bulk susceptibility of the shocked and unshocked Taunus quartzite is in diamagnetic range, with values consistently below -30 X 10^{-6} SI. These negative values are due to the high quartz content, with insignificant amounts of paramagnets and ferromagnets. Notably, the values of the AMS parameters (K_m, P' and T) at the target surface are lower than in the unshocked, while those in the subsurface are higher. This difference between the target surface and the subsurface could either be due to compositional heterogeneity or the effects of the shock wave, as discussed below.

At the target surface, the shock waves travel along the surface, thus, making an angle of c. 39° with the magnetic foliation; while, in the subsurface, below the impact crater, they travel vertically downwards. The shock waves thus make an angle of c. 51° with the magnetic foliation. It may be possible that this acute and obtuse angle subtended by the shock wave propagation direction, and thus by the sigma 1, on the magnetic foliation may provoke different microstructural responses in the quartz due to its crystallographic anisotropy (e.g., Timms et al., 2010). Different effects on magnetic fabrics due to different orientation of shock wave is already well documented for other magnetic carriers, such as the biotite (Amar Agarwal, Kontny, et al., 2019).

The overall quantum of change of AMS parameters is higher in the subsurface than the target surface. This may indicate that in a vertical impact, the highest shock pressure, and thus the damage, is focused below the crater floor and not around the crater wall. A contrary argument could be that the target surface being a free surface may have reduced the damage. However, the lower specimens collected from the target surface (5.13 to 5.24) were not in contact with the free surface. These specimens still show lesser change in the AMS parameters comparted to the subsurface.

4.2 Reorientation of diamagnetic fabrics in the target- and sub-surface

At the target surface, the reorientation of the magnetic fabrics, and thus the damage, is stronger near the crater and decreases with distance (Fig. 7a, b). Furthermore, at both the target- and the sub-surface the reorientation is higher in the upper specimens (5.1 to 5.12 and 6.1 to 6.12) than in the lower (5.13 to 5.24 and 6.13 to 6.21). This is owed to the decreasing intensity of the shock waves with distance from the point source. Note that lower specimens are farther away from the point source than the upper specimens.

After the impact experiment, the magnetic fabrics are more dispersed (Table 1, Fig. 6). Higher dispersion was also reported from impact experiments on Maggia gneiss with magnetite as the predominant magnetic carrier (Amar Agarwal, Kontny, et al., 2019). They attributed the dispersion to fracturing, shearing and kinking of biotite that passively rotated and translated the magnetite grains. In the present case fracturing of the quartz grains may have rotated the grains, thus, increasing the dispersion of the magnetic fabrics. Different principal susceptibility axes behave differently at the target surface and the subsurface, for example, k_1 is most dispersed at the target surface, while k_2 and k_3 are more dispersed in subsurface. This may be another indication of dissimilar effects on magnetic fabrics due to different orientation of shock wave.

In the subsurface, the reorientation, and thus the damage, is concentrated in a zone, ca. 4 d_p wide, directly below the point of impact (Fig. 7c). This is contradictory to the general assumption of concentric zones of shock metamorphic stages, which decrease in intensity with distance from the point of impact

(Kenkmann et al., 2014; Pierazzo & Melosh, 2000). In a previous study, with the impact along the foliation of Maggia gneiss (foliation perpendicular to the target surface), a similar concentration below the point of impact was observed (Amar Agarwal, Kontny, et al., 2019). In the case of Maggia gneiss preferentially aligned biotite provided a strong mechanical anisotropy. Biotite deforms more easily along the basal plane, and thus, the mechanical anisotropy played a crucial role in concentrating the reorientation in a zone below the point of impact. However, quartz has low mechanical anisotropy (Timms et al., 2010). The concentration of damage in a ca. 4 d_p wide zone is, thus, significant.

We look at numerical models, which discuss the effect of low shock pressures in the crater subsurface for the possible reasons of concertation of damage in a narrow zone below the point of impact. Winkler et al. (2018) used 2D ISALE models to estimate total plastic strain in the subsurface of experimentally shocked blocks of Taunus quartzite. They used blocks of 20 X 20 x 20 cm, and a steel projectile of 2.5 mm diameter accelerated to impact speeds of ~5 kms^{-1}. Their block size is same as us, and the projectile parameters are comparable. However, their numerical models show decreasing strain intensity with depth and radial distance from the point of impact. Beyond ca. 4 d_p from the point of impact, their model reveals, thin strongly localized zones of high strain that extend radially into deeper crater subsurface. The subsurface samples investigated in the present study also suffered low shock pressures. However, in the specimens that show largest reorientation of k3, we did not observe such localized zones of high strain. We therefore argue that although the shock waves propagate with hemispherical wave front in the target, the damage was generally concentrated in a zone directly below the point of impact.

5. Conclusions

This paper investigates the capability of diamagnetic fabrics to systematically record the effects of shock waves and the possibility of them being used as a proxy for deformation caused by low shock pressures. An impact experiment was done on a block of Taunus quartzite. The block was sawed in half, and cylindrical specimens were drilled from the target and the sawed surface. The sawed surface represents the subsurface.

Our results show that, firstly, there is a marked increase in the bulk susceptibility in the crater subsurface. Although, post-impact increase in the bulk susceptibility is known from para- and ferro-magnetic rocks, the increase in the diamagnetic susceptibility is a novel observation. This observation is also very interesting, as diamagnetic rocks are considered to be very weakly magnetic. Another interesting observation is that, after impact the value of AMS parameters (P' and T) has increased in the subsurface but lowered in the target surface. k_1 is most dispersed at the target surface, while k_2 and k_3 are more dispersed in subsurface. This may be due to the acute and obtuse angle subtended by the shock wave propagation direction on the magnetic foliation. Further studies are

needed to determine the reason for this increase in the bulk susceptibility and the effects of shock waves traversing at different orientations with respect to the magnetic fabrics.

Secondly, at the target surface, there is a systematically decreasing reorientation of diamagnetic fabrics with distance from the impact crater. This is attributed to the decreasing intensity of shock waves. However, in the subsurface, the reorientation is concentrated in a thin, ca. 4 *dp* wide, zone directly below the point of impact, suggesting that the damage in the subsurface, below the crater floor, is higher than the target surface. Within the subsurface the damage is maximum directly below the point of impact, even though the shock wave propagates hemispherically from the point source.

Finally, the change in AMS parameters and systematic reorientation of the magnetic fabrics highlight the fact that even diamagnetic fabrics can be used as a proxy to the damage and deformation by shock waves. Through future impact experiments with well-defined shock pressures, it may be possible to use the reorientation of magnetic fabrics in quartz as a shock barometer in weakly shocked rocks.

6. Acknowledgements

Pallavi Agarwal is thanked for drilling the specimens from the blocks. Agnes Kontny is thanked for the drilling and AMS measurement facilities at KIT Germany. AA thanks the initiation grant of Indian Institute of Technology-Kanpur and Start-up grant (#SRG/2020/000470) by SERB-DST. ST thanks the department of Earth Sciences, IIT Kanpur, and CSIR-UGC for the scholarship (Ref no.- 408/CSIR-UGC NET JUNE 2019). The cratering experiments have been conducted in the framework of the research unit FOR-887, MEMIN, the Multidisciplinary Experimental and Modeling Impact research Network, financed by the Deutsche Forschungsgemeinschaft DFG, grant KE 732/16-2. We are grateful to the technicians of the Ernst-Mach-Institute for conducting the shots.

7. References

Agarwal, A., & Alva-Valdivia, L. M. (2019). Curie temperature of weakly shocked target basalts at the Lonar impact crater, India. *Earth, Planets and Space*, *71*(1), 141. https://doi.org/10.1186/s40623-019-1120-9Agarwal, Amar, Kontny, A., & Greiling, R. O. (2015). Relationships among magnetic fabrics, microfractures and shock pressures at an impact crater: A case study from Lockne crater, Sweden. *Journal of Applied Geophysics*, *114*, 232–243. https://doi.org/10.1016/j.jappgeo.2015.01.010Agarwal, Amar, Kontny, A., Srivastava, D. C., & Greiling, R. O. (2016). Shock pressure estimates in target basalts of a pristine crater: A case study in the Lonar crater, India. *Geological Society of America Bulletin*, *128*(1–2), B31172.1.

https://doi.org/10.1130/B31172.1Agarwal, Amar, Poelchau, M. H., Kenkmann, T., Rae, A., & Ebert, M. (2019). Impact Experiment on Gneiss: The Effects of Foliation on Cratering Process. *Journal of Geophysical Research: Solid Earth*, *124*(12), 13532–13546. https://doi.org/10.1029/2019JB018345Agarwal, Amar, Kontny, A., Kenkmann, T., & Poelchau, M. H. (2019). Variation in Magnetic Fabrics at Low Shock Pressure Due to Experimental Impact Cratering. *Journal of Geophysical Research: Solid Earth*, *124*(8), 9095–9108. https://doi.org/10.1029/2018JB017128Agarwal, Amar, Srivastava, D. C., Shah, J., & Mamtani, M. A. (2021). Magnetic fabrics in an apparently undeformed granite body near Main Boundary Thrust (MBT), Kumaun Lesser Himalaya, India. *Tectonophysics*, *815*, 228996. https://doi.org/10.1016/j.tecto.2021.228996Ahrens, T. J., & Rubin, A. M. (1993). Impact-induced tensional failure in rock. *Journal of Geophysical Research: Planets*, *98*(92), 1185–1203. https://doi.org/10.1029/92JE02679Alva-Valdivia, L. M., Cyphers, A., De La Luz Rivas-Sánchez, M., Agarwal, A., Zurita-Noguera, J., & Urrutia-Fucugauchi, J. (2017). Mineralogical and magnetic characterization of Olmec ilmenite multi-perforated artifacts and inferences on source provenance. *European Journal of Mineralogy*, *29*(5), 851–860. https://doi.org/10.1127/ejm/2017/0029-2654Alva-Valdivia, L. M., Rodríguez-Trejo, A., Morales, J., González-Rangel, J. A., & Agarwal, A. (2019). Paleomagnetism and age constraints of historical lava flows from the El Jorullo volcano, Michoacán, Mexico. *Journal of South American Earth Sciences*, *93*, 439–448. https://doi.org/10.1016/j.jsames.2019.05.016Birkhoff, G., MacDougall, D. P., Pugh, E. M., Taylor, G., & Taylor, S. G. (1948). Explosives with lined cavities. *Journal of Applied Physics*, *19*(6), 563–582. https://doi.org/10.1063/1.1698173Borradaile, G., & Alford, C. (1987). Relationship between magnetic susceptibility and strain in laboratory experiments. *Tectonophysics*, *133*(1–2), 121–135. https://doi.org/10.1016/0040-1951(87)90285-XBorradaile, G.J., & Henry, B. (1997). Tectonic applications of magnetic susceptibility and its anisotropy. *Earth-Science Reviews*, *42*(1–2), 49–93. https://doi.org/10.1016/S0012-8252(96)00044-XBorradaile, G J. (1987). Analysis of strained sedimentary fabrics: review and tests. *Canadian Journal of Earth Sciences*, *24*(3), 442–455.Borradaile, Graham J., & Tarling, D. H. (1981). The influence of deformation mechanisms on magnetic fabrics in weakly deformed rocks. *Tectonophysics*, *77*(1–2), 151–168. https://doi.org/10.1016/0040-1951(81)90165-7Borradaile, Graham John. (1988). Magnetic susceptibility, petrofabrics and strain. *Tectonophysics*, *156*(1–2), 1–20. https://doi.org/10.1016/0040-1951(88)90279-XBurmeister, K. C., Harrison, M. J., Marshak, S., Ferré, E. C., Bannister, R. A., & Kodama, K. P. (2009). Comparison of Fry strain ellipse and AMS ellipsoid trends to tectonic fabric trends in very low-strain sandstone of the Appalachian fold–thrust belt. *Journal of Structural Geology*, *31*(9), 1028–1038.Cardozo, N., & Allmendinger, R. W. (2013). Spherical projections with OSXStereonet. *Computers & Geosciences*, *51*, 193–205. https://doi.org/10.1016/j.cageo.2012.07.021Cifelli, F., Mattei, M., Hirt, A. M., & Günther, A. (2004). The origin of tectonic fabrics in "undeformed" clays: The

early stages of deformation in extensional sedimentary basins. *Geophysical Research Letters*, *31*(9), n/a-n/a. https://doi.org/10.1029/2004GL019609Cockell, C. S., & Lee, P. (2002). The biology of impact craters - A review. *Biological Reviews of the Cambridge Philosophical Society*, *77*(3), 279–310. https://doi.org/10.1017/S146479310100584XDay, R., Fuller, M., & Schmidt, V. A. (1977). Hysteresis properties of titanomagnetites: Grain-size and compositional dependence. *Physics of the Earth and Planetary Interiors*, *13*(4), 260–267. https://doi.org/10.1016/0031-9201(77)90108-XElbra, T., Kontny, A., & Pesonen, L. (2009). Rock-magnetic properties of the ICDP-USGS Eyreville core, Chesapeake Bay impact structure, Virginia, USA. *Geological Society of America*, *80301*(303), 119–135. https://doi.org/10.1130/2009.2458(06)Ferré, E. C. (2002). Theoretical models of intermediate and inverse AMS fabrics. *Geophysical Research Letters*, *29*(7), 29–32. https://doi.org/10.1029/2001GL014367Ferré, E. C., Gébelin, A., Till, J. L., Sassier, C., & Burmeister, K. C. (2014). Deformation and magnetic fabrics in ductile shear zones: A review. *Tectonophysics*, *629*(C), 179–188. https://doi.org/10.1016/j.tecto.2014.04.008Fisher, N. I., Lewis, T., & Embleton, B. J. J. (1993). *Statistical analysis of spherical data*. Cambridge university press.French, B. M., & Koeberl, C. (2010). The convincing identification of terrestrial meteorite impact structures: What works, what doesn't, and why. *Earth-Science Reviews*, *98*(1–2), 123–170. https://doi.org/10.1016/j.earscirev.2009.10.009Gattacceca, J., Lamali, A., Rochette, P., Boustie, M., & Berthe, L. (2007). The effects of explosive-driven shocks on the natural remanent magnetization and the magnetic properties of rocks. *Physics of the Earth and Planetary Interiors*, *162*(1–2), 85–98. https://doi.org/10.1016/j.pepi.2007.03.006Grajales-Nishimura, J. M., Cedillo-Pardo, E., Rosales-Domínguez, C., Morán-Zenteno, D. J., Alvarez, W., Claeys, P., et al. (2000). Chicxulub impact: The origin of reservoir and seal facies in the southeastern Mexico oil fields. *Geology*, *28*(4), 307–310.Greeley, R., Fink, J., Gault, D. E., Snyder, D. B., Guest, J., & Schultz, P. H. (1980). Impact cratering in viscous targets: Laboratory experiments. Pergamon Press.Greeley, R., Fink, J. H., Gault, D. E., & Guest, J. E. (1982). *Experimental simulation of impact cratering on icy satellites. Satellites of Jupiter*.Grieve, R. A. F., & Masaitis, V. L. (1994). The economic potential of terrestrial impact craters. *International Geology Review*, *36*(2), 105–151.Grieve, Richard A F. (2005). Economic natural resource deposits at terrestrial impact structures. *Geological Society, London, Special Publications*, *248*(1), 1–29.Hirt, A.M., Lowrie, W., Clendenen, W. S., & Kligfield, R. (1993). Correlation of strain and the anisotropy of magnetic susceptibility in the Onaping Formation: evidence for a near-circular origin of the Sudbury Basin. *Tectonophysics*, *225*(4), 231–254. https://doi.org/10.1016/0040-1951(93)90300-9Hirt, Ann M., & Almqvist, B. S. G. (2012). Unraveling magnetic fabrics. *International Journal of Earth Sciences*, *101*(3), 613–624. https://doi.org/10.1007/s00531-011-0664-0Hrouda, F. (2004). Problems in interpreting AMS parameters in diamagnetic rocks. *Geological Society Special Publication*, *238*(2), 49–59. https://doi.org/10.1144/GSL.SP.2004.238.01.05Hrouda, F., & Kapička, A. (1986). The effect of quartz on the magnetic anisotropy of quartzite. *Studia Geo-*

physica et Geodaetica, *30*(1), 39–45. https://doi.org/10.1007/BF01630853Jelinek, V. (1981). Characterization of the magnetic fabric of rocks. *Tectonophysics*, *79*(3), T63–T67. Retrieved from http://www.sciencedirect.com/science/article/pii/0040195181901104Kenkmann T., Poelchau, M. H., & Wulf, G. (2014). Structural geology of impact craters. *Journal of Structural Geology*, *62*, 156–182. https://doi.org/10.1016/j.jsg.2014.01.015Kenkmann, T., Deutsch, A., Thoma, K., Ebert, M., Poelchau, M. H., Buhl, E., et al. (2018). Experimental impact cratering: A summary of the major results of the MEMIN research unit. *Meteoritics & Planetary Science*, *53*(8), 1543–1568. https://doi.org/10.1111/maps.13048Kenkmann, T., Wulf, G., & Agarwal, A. (2020). Ramgarh, Rajasthan, India: A 10 km diameter complex impact structure. *Meteoritics & Planetary Science*, *55*(4), 936–961. https://doi.org/10.1111/maps.13454Kieffer, S. W. (1971). Shock metamorphism of the Coconino sandstone at Meteor Crater, Arizona. *Journal of Geophysical Research*, *76*(23), 5449–5473. Retrieved from http://onlinelibrary.wiley.com/doi/10.1029/JB076i023p05449/fullKissel, C., Barrier, E., Laj, C., & Lee, T. (1986). Magnetic fabric in "undeformed" marine clays from compressional zones. *Tectonics*, *5*(5), 769–781.Lange, M. A., Ahrens, T. J., & Boslough, M. B. (1984). Impact cratering and spall failure of gabbro. *Icarus*, *58*(3), 383–395.Lüneburg, C. M., Lampert, S. A., Lebit, H. D., Hirt, A. M., Casey, M., & Lowrie, W. (1999). Magnetic anisotropy, rock fabrics and finite strain in deformed sediments of SW Sardinia (Italy). *Tectonophysics*, *307*(1–2), 51–74.Masaitis, V. L. (1998). Popigai crater: Origin and distribution of diamond-bearing impactites. *Meteoritics & Planetary Science*, *33*(2), 349–359.Melosh, H. J. (1980). Cratering mechanics—Observational, experimental, and theoretical. *Annual Review of Earth and Planetary Sciences*, *8*(1), 65–93.Moser, D., Güldemeister, N., Wünnemann, K., & Grosse, C. (2013). Acoustic emission analysis of experimental impact processes in comparison to ultrasound measurements and numerical modeling. *Journal of Acoustic Emission (JAE)*, *31*(1), 50–66.Muxworthy, A. R., Bland, P. A., Davison, T. M., Moore, J., Collins, G. S., & Ciesla, F. J. (2017). Evidence for an impact-induced magnetic fabric in Allende, and exogenous alternatives to the core dynamo theory for Allende magnetization. *Meteoritics & Planetary Science*, *52*(10), 2132–2146. https://doi.org/10.1111/maps.12918Nishioka, I, & Funaki, M. (2008). Irreversible changes in anisotropy of magnetic susceptibility. Study of basalts from lunar crater and experimentally impacted basaltic andesite. In *71st Annual Meteoritical Society Meeting* (p. 5207). Matsue, Japan: METEORITICAL SOC.Nishioka, Itoyuki, Funaki, M., & Sekine, T. (2007). Shock-induced anisotropy of magnetic susceptibility: Impact experiment on basaltic andesite. *Earth, Planets and Space*, *59*(12), 45–48. https://doi.org/10.1186/BF03352060Oberbeck, V. R. (1971). Laboratory simulation of impact cratering with high explosives. *Journal of Geophysical Research*, *76*(23), 5732–5749.Parés, J. M. (2004). How deformed are weakly deformed mudrocks? Insights from magnetic anisotropy. *Geological Society, London, Special Publications*, *238*(1), 191–203. https://doi.org/10.1144/GSL.SP.2004.238.01.13Passchier, C. W., & Trouw, R. A. J. (2005). *Microtectonics* (2nd ed.). Berlin: Springer.Pierazzo, E., &

Melosh, H. J. (2000). Understanding Oblique Impacts from Experiments, Observations, and Modeling. *Annual Review of Earth and Planetary Sciences*, *28*(1), 141–167. https://doi.org/10.1146/annurev.earth.28.1.141Poelchau, M. H., Kenkmann, T., Hoerth, T., Schäfer, F., Rudolf, M., & Thoma, K. (2014). Impact cratering experiments into quartzite, sandstone and tuff: The effects of projectile size and target properties on spallation. *Icarus*, *242*, 211–224. https://doi.org/10.1016/j.icarus.2014.08.018Pohl, J., Stöffler, D., Gall, H., & Ernstson, K. (1977). Ries Impact Crater. In *Impact and explosion cratering* (pp. 343–404). new york: Pergamon Press.Reimold, W. U., Koeberl, C., Gibson, R. L., & Dressler, B. O. (2005). Economic Mineral Deposits in Impact Structures: A Review. In C. Koeberl & H. Henkel (Eds.), *Impact Tectonics* (pp. 479–552). Berlin/Heidelberg: Springer-Verlag. https://doi.org/10.1007/3-540-27548-7_20Rochette, P. (1987). Magnetic susceptibility of the rock matrix related to magnetic fabric studies. *Journal of Structural Geology*, *9*(8), 1015–1020. https://doi.org/10.1016/0191-8141(87)90009-5Schneider, E., & Schäfer, F. (2001). Hypervelocity impact research-acceleration technology and applications. *Advances in Space Research*, *28*(9), 1417–1424.Schultz, P. H., Eberhardy, C. a., Ernst, C. M., A'Hearn, M. F., Sunshine, J. M., & Lisse, C. M. (2007). The Deep Impact oblique impact cratering experiment. *Icarus*, *191*, 84–122. https://doi.org/10.1016/j.icarus.2007.06.031Scott, R., & Spray, J. (1999). Magnetic fabric constraints on friction melt flow regimes and ore emplacement direction within the South Range Breccia Belt, Sudbury Impact Structure. *Tectonophysics*, *307*(1–2), 163–189. Retrieved from http://www.sciencedirect.com/science/article/pii/S0040195199001249Soto, R., Larrasoaña, J. C., Arlegui, L. E., Beamud, E., Oliva-Urcia, B., & Simón, J. L. (2009). Reliability of magnetic fabric of weakly deformed mudrocks as a palaeostress indicator in compressive settings. *Journal of Structural Geology*, *31*(5), 512–522. https://doi.org/10.1016/j.jsg.2009.03.006Stöffler, D. (1972). Deformation and transformation of rock-forming minerals by natural and experimental shock processes. I-Behavior of minerals under shock compression. *Fortschritte Der Mineralogie*, *49*, 64.Stöffler, Dieter, & Langenhorst, F. (1994). Shock metamorphism of quartz in nature and experiment: I. Basic observation and theory*. *Meteoritics*, *29*(2), 155–181.Stöffler, Dieter, Hamann, C., & Metzler, K. (2018). Shock metamorphism of planetary silicate rocks and sediments: Proposal for an updated classification system. *Meteoritics & Planetary Science*, *53*(1), 5–49. https://doi.org/10.1111/maps.12912Tarling, D. H., & Shi, H. (1995). Magnetic anisotropy of borehole core samples. *Geological Society Special Publication*, *98*(98), 273–280. https://doi.org/10.1144/GSL.SP.1995.098.01.18Tauxe, L. (2003). *Paleomagnetic Principles and Practice* (1st ed., Vol. 17). Dordrecht: Kluwer Academic Publishers. https://doi.org/10.1007/0-306-48128-6Timms, N. E., Healy, D., Reyes-Montes, J. M., Collins, D. S., Prior, D. J., & Young, R. P. (2010). Effects of crystallographic anisotropy on fracture development and acoustic emission in quartz. *Journal of Geophysical Research*, *115*(B7), B07202. https://doi.org/10.1029/2009JB006765Urrutia-Fucugauchi, J., Delgadillo-Peralta, M., Pérez-Cruz, L., & Velasco-Villarreal, M. (2012).

Heating-induced changes in the anisotropy of magnetic susceptibility of impact breccias, Chicxulub Crater (Mexico). *Studia Geophysica et Geodaetica*, *56*(3), 769–787. https://doi.org/10.1007/s11200-010-0292-3Winkler, R., Luther, R., Poelchau, M. H., Wünnemann, K., & Kenkmann, T. (2018). Subsurface deformation of experimental hypervelocity impacts in quartzite and marble targets. *Meteoritics & Planetary Science*, *53*(8), 1733–1755. https://doi.org/10.1111/maps.13080Yokoyama, E., Trindade, R. I. F., Lana, C., Filho, C. R. S., Baratoux, D., Marangoni, Y. R., & Tohver, E. (2012). Magnetic fabric of Araguainha complex impact structure (Central Brazil): Implications for deformation mechanisms and central uplift formation. *Earth and Planetary Science Letters*, *331–332*, 347–359. https://doi.org/10.1016/j.epsl.2012.01.005